

Design and Synthesis of 2-Heterocyclyl-3-arylthio-1*H*-indoles as Potent Tubulin Polymerization and Cell Growth Inhibitors with Improved Metabolic Stability

Giuseppe La Regina,[†] Ruoli Bai,[‡] Willeke Rensen,[§] Antonio Coluccia,[†] Francesco Piscitelli,[†] Valerio Gatti,[†] Alessio Bolognesi,[§] Antonio Lavecchia,[#] Ilaria Granata,^{||} Amalia Porta,^{||} Bruno Maresca,^{||} Alessandra Soriani,[∇] Maria Luisa Iannitto,[∇] Marisa Mariani,[○] Angela Santoni,^{∇,§} Andrea Brancale,[⊥] Cristiano Ferlini,[○] Giulio Dondio,[◆] Mario Varasi,[¶] Ciro Mercurio,[□] Ernest Hamel,[‡] Patrizia Lavia,[§] Ettore Novellino,[#] and Romano Silvestri^{*,†}

[†]Istituto Pasteur—Fondazione Cenci Bolognetti, Dipartimento di Chimica e Tecnologie del Farmaco, Sapienza Università di Roma, Piazzale Aldo Moro 5, I-00185 Roma, Italy

[‡]Screening Technologies Branch, Developmental Therapeutics Program, Division of Cancer Treatment and Diagnosis, National Cancer Institute at Frederick, National Institutes of Health, Frederick, Maryland 21702, United States

[§]CNR, National Research Council, Institute of Molecular Biology and Pathology, Sapienza Università di Roma, Via degli Apuli 4, I-00185 Roma, Italy

^{||}Dipartimento di Scienze Farmaceutiche, Sezione Biomedica, Università di Salerno, Via Ponte don Melillo, I-84084 Fisciano, Salerno, Italy

[⊥]Welsh School of Pharmacy, Cardiff University, King Edward VII Avenue, Cardiff, CF10 3NB, U.K.

[#]Dipartimento di Chimica Farmaceutica e Tossicologica, Università di Napoli Federico II, Via Domenico Montesano 49, I-80131, Napoli, Italy

[∇]Dipartimento di Medicina Sperimentale e Patologia, Sapienza Università di Roma, Viale Regina Elena 324, I-00161 Roma, Italy

[○]Danbury Hospital Research Institute, Tumor Reproductive Biology Research Laboratory, 131 West Street, Danbury, Connecticut 06810, United States

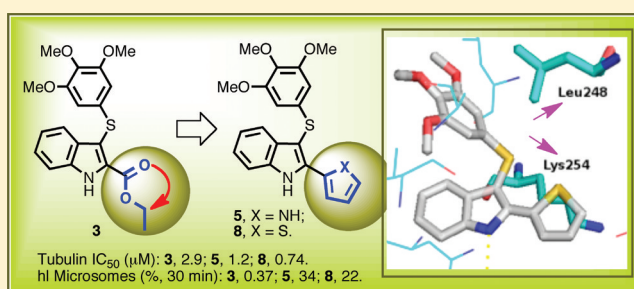
[◆]NiKem Research Srl, Via Zambelletti 25, 20021 Baranzate, Milano, Italy

[¶]European Institute of Oncology, Via Adamello 16, 20139 Milan, Italy

[□]Genextra Group, DAC SRL, Via Adamello 16, 20139 Milan, Italy

Supporting Information

ABSTRACT: New arylthioindoles (ATIs) were obtained by replacing the 2-alkoxycarbonyl group with a bioisosteric 5-membered heterocycle nucleus. The new ATIs **5**, **8**, and **10** inhibited tubulin polymerization, reduced cell growth of a panel of human transformed cell lines, and showed higher metabolic stability than the reference ester **3**. These compounds induced mitotic arrest and apoptosis at a similar level as combretastatin A-4 and vinblastine and triggered caspase-3 expression in a significant fraction of cells in both p53-proficient and p53-defective cell lines. Importantly, ATIs **5**, **8**, and **10** were more effective than vinorelbine, vinblastine, and paclitaxel as growth inhibitors of the P-glycoprotein-overexpressing cell line NCI/ADR-RES. Compound **5** was shown to have medium metabolic stability in both human and mouse liver microsomes, in contrast to the rapidly degraded reference ester **3**, and a pharmacokinetic profile in the mouse characterized by a low systemic clearance and excellent oral bioavailability.



INTRODUCTION

Microtubules (MTs) are a broadly exploited target in the search for new effective anticancer agents.^{1–3} MTs are highly dynamic cylindrical structures principally composed of α , β -tubulin heterodimers. During their assembly, MTs continuously undergo regulated transitions between polymerization and

depolymerization, a process known as dynamic instability. MTs are required for many essential cellular functions, including the maintenance of cell shape, cell motility, intracellular transport,

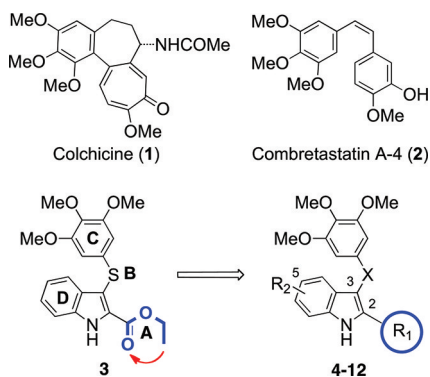
Received: June 25, 2011

Published: November 1, 2011

and cell division. At the onset of mitosis, the interphase MTs rapidly disassemble, and newly polymerized MTs organize into the mitotic spindle, a symmetrical dynamic structure that drives chromosome segregation. Thus, the mitotic apparatus is cyclically assembled to ensure even chromosome distribution into two genetically identical daughter cells. Interfering with MT function, by either inhibiting tubulin polymerization or blocking MT dynamic transitions, causes cell damage and blocks cell division. Devising compounds that interfere with these cellular processes is therefore an established strategy to inhibit the proliferation of cancer cells.^{2–4}

MT assembly can be inhibited by using colchicine (**1**),^{5,6} combretastatin A-4 (CSA4, **2**)⁷ (Chart 1), and the *Cathar-*

Chart 1. Structures of ATI Derivatives 3–12 and Reference Compounds 1 and 2^a



^aA–D: ATIs' binding regions. R₁ = 1*H*-pyrrol-2-yl, 1*H*-pyrrol-3-yl, furan-2-yl, furan-3-yl, thiophen-2-yl, thiophen-3-yl; R₂ = H, OMe; X = S, C=O, CH₂.

anthus alkaloids vincristine and vinblastine (VBL), all of which prevent tubulin polymerization. This results in MT destabilization, arrest of mitotic progression, and subsequent cell death. Another class of antimetabolic drugs, including taxoids and epothilones, target a luminal site on the β -subunit^{8,9} and enter the lumen through a binding site¹⁰ located at a pore on the MT surface formed by different tubulin heterodimers. In that group, paclitaxel (PTX) stimulates MT polymerization and stabilization at high concentrations, whereas at lower concentrations it inhibits MT dynamics with little effect on the proportion of tubulin in polymer.¹¹ Thus, either inhibition or enhancement of tubulin assembly prevents proper functioning of the mitotic apparatus and ultimately blocks cell division.

MT-targeting drugs with different mechanisms of action have an empirical therapeutic efficacy in a variety of tumor types. Nevertheless, a number of unsolved problems still remain in their clinical use: (i) drug resistance appears often, with a poorly understood molecular basis, which makes it a difficult to predict phenomenon; (ii) secondary toxicity on nontransformed cells is often observed in clinical practice, partly independent of the antitubulin mechanism of action of any specific drug.¹² There is therefore an urgent need to design and synthesize novel tubulin inhibitors of improved efficacy.¹³

Arylthioindole (ATI) antimetabolic agents are potent inhibitors of tubulin polymerization and cancer cell growth. ATIs inhibit [³H]colchicine binding in the β -tubulin site close to its interface with α -tubulin within the α , β -dimer.¹⁴ Structure–activity relationship (SAR) studies of ATIs^{14–17} have been focused on the following: (A) the substituent at position 2 of the indole,

(B) the sulfur atom bridge, (C) the 3-arylthio group, and (D) the substituent at position 5 of the indole (Chart 1). Previous SAR studies at the A region addressed the elongation of the 2-methoxy- or 2-ethoxycarbonyl group by means of C3–C5 alkoxy chains.^{14,15} Other ester functionalities were not explored, as the C3–C5 alkoxy chains led to decreases of both antitubulin and antiproliferative activities.¹⁵

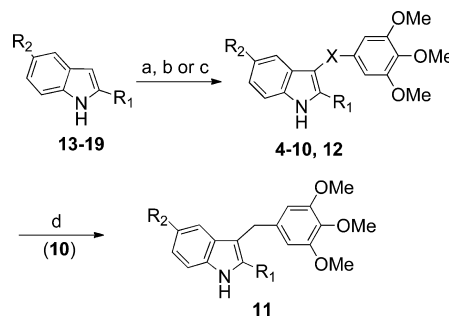
In studies to be presented here, we found that ester derivative **3** was extensively degraded by mouse and human liver microsomes. Therefore, we decided to replace the ethoxycarbonyl group of **3** (A region) with a potentially more stable five-membered heterocyclic nucleus, the bioisosteric pyrrole, furan, and thiophene moieties.¹⁸ Preliminary modeling studies showed that, with respect to the small/medium linear chain,¹⁵ the five-membered heterocycle at position 2 of the indole nucleus could form new hydrophobic interactions with Lys254 and Leu248 of the colchicine site of tubulin (Supporting Information).

Here, we report that this strategy was successful. The analogues with a pyrrole (**4**, **5**), furan (**6**, **7**), or thiophene (**8**–**12**) moiety had enhanced activity against the target tubulin, and moreover, compound **5**, in particular, displayed much better stability than **3** in the microsomal assays and good pharmacokinetic properties.

CHEMISTRY

Microwave (MW) reaction of an appropriate 2-heterocyclyl-1*H*-indole **13**,¹⁹ **14**–**17**, or **19** with bis(3,4,5-trimethoxyphenyl)disulfide¹³ in the presence of sodium hydride in anhydrous DMF at 110 °C (150 W) for 2 min furnished **4**–**8** or **12** (Scheme 1).

Scheme 1. Synthesis of Compounds 4–12^a



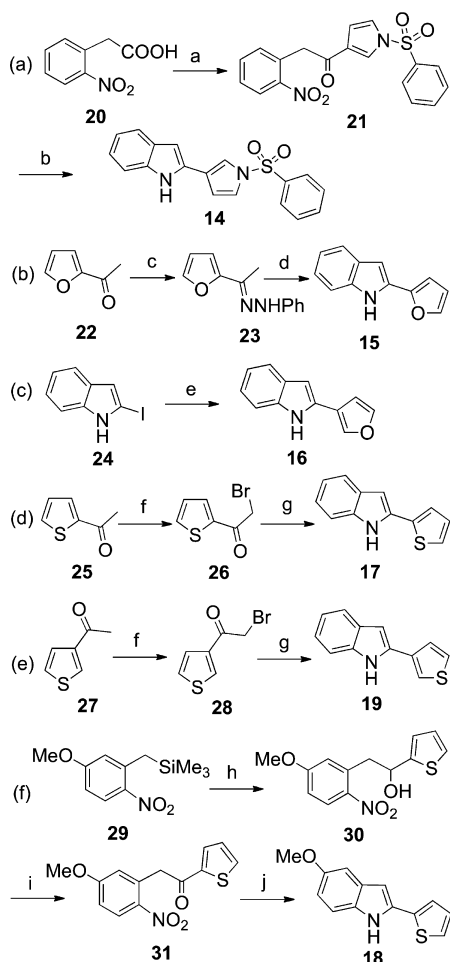
^a**4**–**12**; see Table 1. **13**:²⁴ R₁ = 1*H*-pyrrol-2-yl, R₂ = H. **14**: R₁ = 1-(benzenesulfonyl)-1*H*-pyrrol-3-yl, R₂ = H. **15**: R₁ = furan-2-yl, R₂ = H. **16**: R₁ = furan-3-yl, R₂ = H. **17**: R₁ = thiophen-2-yl, R₂ = H. **18**: R₁ = thiophen-2-yl, R₂ = OMe. **19**: R₁ = thiophen-3-yl, R₂ = H. Reagents and reaction conditions: (a) (for **4**–**8** and **12**) (i) NaH, anhydrous DMF, 25 °C, 10 min; (ii) bis(3,4,5-trimethoxyphenyl)disulfide, closed vessel, 150 W, 110 °C, 2 min, yield 10–83%; (b) (for **9**) (i) NaH, anhydrous DMF, 0 °C, Ar stream, 15 min; (ii) bis(3,4,5-trimethoxyphenyl)disulfide, 110 °C, Ar stream, overnight, yield 70%; (c) (for **10**) 3,4,5-trimethoxybenzoyl chloride, anhydrous AlCl₃, 1,2-dichloroethane, closed vessel, 150 W, 110 °C, 2 min, yield 34%; (d) (for **11**) NaBH₄ (10 equiv), ethanol, reflux, 2.5 h, yield 21%.

Compound **10** was prepared from **17** and 3,4,5-trimethoxybenzoyl chloride in the presence of anhydrous aluminum chloride in 1,2-dichloroethane at 110 °C (150 W) for 2 min. Sodium borohydride (10 equiv) reduction of **10** in boiling ethanol provided **11**. Derivative **9** was obtained by heating the

corresponding indole **18** with the disulfide¹³ in the presence of sodium hydride in anhydrous DMF.

The acid chloride of **20** was treated with 1-(phenylsulfonyl)-1*H*-pyrrole in the presence of anhydrous aluminum chloride to give the intermediate **21**, which underwent intramolecular cyclization to **14** with iron powder in glacial acetic acid at 60 °C (Scheme 2a). Treatment of 2-acetylthiophene with phenylhydrazine

Scheme 2. Synthesis of Compounds 14–19^a



^aReagents and conditions: (a) (i) oxalylchloride, catalytic anhydrous DMF, 1,2-dichloroethane, 0 °C, Ar stream, 30 min; (ii) 1-(phenylsulfonyl)-1*H*-pyrrole, AlCl₃, 0 °C, Ar stream, 15 min, yield 10%; (b) Fe, AcOH, 60 °C, overnight, yield 10%; (c) phenylhydrazine hydrochloride, anhydrous CH₃COONa, ethanol, open vessel, 250 W, PowerMAX, 80 °C, 5 min, yield 94%; (d) PPA, 110 °C, 1 h, yield 55%; (e) 3-furan boronic acid pinacol ester, Pd(II) acetate, potassium carbonate, 1-methyl-2-pyrrolidinone/water, closed vessel, 200 W, 110 °C, 15 min, yield 95%; (f) bromine, dichloromethane, 25 °C, 1 h, yield 57–80%; (g) (i) aniline, 25 °C, 3 h; (ii) catalytic anhydrous DMF, closed vessel, 150 W, 100 °C, 1 min, yield 16–40%; (h) thiophen-2-carboxaldehyde, TBAF, anhydrous THF, 25 °C, Ar stream, 15 min, yield 61%; (i) pyridinium chlorochromate, anhydrous CH₂Cl₂, 25 °C, 1.5 h, yield 56%; (j) tin(II) chloride dihydrate, AcOEt, reflux, 3 h, yield 21%.

hydrochloride in the presence of anhydrous sodium acetate in an open vessel at 80 °C (250 W) for 5 min furnished hydrazone **23**, which was converted to **15** by heating at 110 °C with polyphosphoric acid (PPA) for 1 h (Scheme 2b). Reaction of 2-iodo-1*H*-indole²⁰ (**24**) with the pinacol ester of furan-3-boronic

acid in the presence of Pd(II) acetate and potassium carbonate in a closed vessel at 110 °C (200 W) for 15 min gave **16** (Scheme 2c).

2-Acetyl- (**25**) and 3-acetylthiophene (**27**) were brominated to **26** and **28** and transformed into **17** or **19**, respectively, by reaction with aniline in the presence of a catalytic amount of DMF in a closed vessel at 100 °C (150 W) for 1 min (Scheme 2d and e). Reaction of (5-methoxy-2-nitrobenzyl)-trimethylsilane²¹ (**29**) with thiophen-2-carboxaldehyde in the presence of tetrabutylammonium fluoride (TBAF) provided alcohol **30**, which was oxidized to **31** with pyridinium chlorochromate. Tin(II) chloride reduction of **31** and subsequent intramolecular cyclization of the amino intermediate furnished **18** (Scheme 2f).

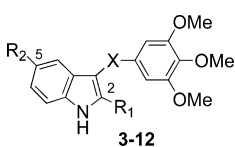
RESULTS AND DISCUSSION

Inhibition of Tubulin Polymerization. In a first set of experiments, we assessed the ability of ATIs **4**–**12** to inhibit tubulin polymerization *in vitro* (Table 1). The new ATIs inhibited tubulin polymerization with IC₅₀ values ranging from 0.74 to 1.9 μM, as compared with 1.0 μM for CSA4 (**2**), 3.2 μM for colchicine (**1**), and 2.9 μM for compound **3**.¹⁴ As tubulin polymerization inhibitors, **6**–**10** and **12** were equal to or more potent than **2**, with the most potent inhibitor being **8**, which had an IC₅₀ of 0.74 μM. Replacement of the sulfur bridging atom of **8** with a carbonyl functionality led to ketone **10**, which inhibited tubulin polymerization with an IC₅₀ of 1.0 μM.

The new ATIs were also examined for potential inhibition of the binding of [³H]colchicine to tubulin (Table 1). All except **11** were strong inhibitors of the binding reaction (75–92% inhibition, although not quite as potent as CSA4). In this assay, the strongest inhibition was observed with compounds **4** and **7**.

Cell Growth Inhibition. All the new ATIs, except compound **11**, inhibited the growth of human MCF-7 nonmetastatic breast cancer epithelial cells with IC₅₀ values ranging from 18 to 60 nM, with the most active compounds being **4** and **5** (Table 1). The antiproliferative effect of compounds **5** and **8**–**11** was evaluated in four additional cancer cell lines in comparison with **2** and doxorubicin (DOX), a DNA-targeting drug often employed in association with antimetabolic agents (Table 2). Compounds **8** and **10** were generally 1 order of magnitude more potent as growth inhibitors of HeLa (cervix), PC3 (prostate), HT-29 (colon), A549 (nonsmall cell lung), and 231-MDA (metastatic breast) carcinoma-derived cell lines as compared with DOX. The effect of **9** went from 2- to 3-fold more potent than DOX to equimolar, depending on the cell line.

Compound **5** was highly effective in the HT-29 and A549 cell lines and had efficacy comparable with that of **9** in the HeLa and PC3 cell lines. As growth inhibitors of HeLa and PC3 cells, compounds **8** and **10** were more potent than **2**, while **5** and **9** were generally less potent. As compared with **2**, compounds **5** and **8**–**11** were superior as inhibitors of the growth of HT-29 and A549 cell lines. Compound **11** was generally comparable with DOX, but it was less potent than **2** as inhibitor of HeLa and PC3 cells growth. These data underscore the effectiveness of ATIs **5** and **8**–**10** in transformed cell types. Such results also highlighted a differential sensitivity to MT-targeting drugs displayed by cell lines with different genetic backgrounds, consistent with results obtained with other drugs that target the mitotic apparatus.^{22,23}

Table 1. Inhibition of Tubulin Polymerization, Growth of MCF-7 Human Breast Carcinoma Cells, and Colchicine Binding by Compounds 1–12


Compd	R ₁	R ₂	X	Tubulin Assembly ^a IC ₅₀ ± SD (μM)	MCF-7 ^b IC ₅₀ ± SD (nM)	Inhibition of Colchicine Binding ^c (% ± SD)
4		H	S	1.1 ± 0.05	18 ± 6	92 ± 0.6
5		H	S	1.2 ± 0.2	20 ± 0	85 ± 1
6		H	S	1.0 ± 0.1	45 ± 4	80 ± 1
7		H	S	1.0 ± 0.1	33 ± 5	93 ± 4
8		H	S	0.74 ± 0.05	39 ± 10	88 ± 2
9		OMe	S	0.98 ± 0.08	58 ± 4	86 ± 2
10		H	C=O	1.0 ± 0.1	36 ± 6	75 ± 3
11		H	CH ₂	1.9 ± 0.2	200	48 ± 5
12		H	S	0.91 ± 0.2	60 ± 20	85 ± 0.4
1	-	-	-	3.2 ± 0.4	5 ± 1	-
2	-	-	-	1.0 ± 0.1	13 ± 3	99 ± 0.3
3 ^d	COOEt	H	S	2.9 ± 0.1	40 ± 2	51 ± 3

^aInhibition of tubulin polymerization. Tubulin was 10 μM during polymerization. ^bInhibition of growth of MCF-7 human breast carcinoma cells.

^cInhibition of [³H]colchicine binding; tubulin was at 1 μM, both [³H]colchicine and inhibitor were at 5 μM. ^dReference 11.

Table 2. Inhibition of Growth of HeLa, PC3, HT29, and A549 Cell Lines by Compounds 5 and 8–11^{a,b}

compd	IC ₅₀ ± SD (μM)			
	HeLa	PC3	HT-29	A549
5	0.4 ± 0.02	0.5 ± 0.1	0.1 ± 0.03	0.08 ± 0.02
8	0.09 ± 0.002	0.2 ± 0.05	0.15 ± 0.03	0.09 ± 0.02
9	0.4 ± 0.02	0.8 ± 0.08	0.4 ± 0.02	0.3 ± 0.09
10	0.07 ± 0.004	0.1 ± 0.08	0.08 ± 0.01	0.08 ± 0.01
11	1 ± 0.03	2 ± 0.1	1 ± 0.05	2 ± 0.08
2	0.2 ± 0.005	0.4 ± 0.02	>10	>10
DOX ^c	1.5 ± 0.03	1.7 ± 0.02	1.0 ± 0.04	1.0 ± 0.08

^aGrowth inhibition of the indicated cell lines (MTT method); incubation time was 48 h. ^bPlots of 231-MDA and A549 cell growth inhibition by compounds 5 and 8–10 are shown in Figures 1S–4S of the Supporting Information. ^cDoxorubicin as reference compound.

We analyzed growth inhibition in an ovarian cancer model with high drug sensitivity (A2780wt), its cisplatin-resistant counterpart (A2780-CIS), and a cell line derived from a cisplatin-resistant patient (OVCAR-3) (Table 3). For the acquired cisplatin-resistance (RI-1) model, compounds 5 and 10 yielded even lower IC₅₀ values than in the parental line, in contrast to the almost 20-fold resistance to cisplatin. On the

Table 3. Growth Inhibition in A2780wt Cells, Its Cisplatin Resistant Counterpart A2780-CIS, and OVCAR-3 by Compounds 5 and 10

compd	IC ₅₀ ± SD (nM)				
	A2780wt	A2780-CIS	OVCAR-3	RI-1 ^a	RI-2 ^b
5	21.5 ± 1.2	6.3 ± 1.8	81 ± 21	0.29	3.8
10	30.5 ± 0.7	29.3 ± 3.2	117 ± 18	0.96	3.8
cisplatin	485 ± 60	8980 ± 565	1816 ± 254	18.5	3.7

^aRI-1 (Resistant Index-1) was calculated by dividing the IC₅₀ obtained in A2780-CIS by the IC₅₀ obtained in A2780wt. ^bRI-2 (Resistant Index-2) was calculated by dividing the IC₅₀ obtained in OVCAR-3 by the IC₅₀ obtained in A2780wt. A value >1 or <1 means either increased cisplatin-resistance or sensitivity, respectively.

other hand, such an increase was not detectable in the endogenous resistance model, as the resistance values (RI-2) for the two ATIs were essentially identical to that obtained with cisplatin in OVCAR-3.

Pgp Overexpressing MDR Cell Lines. Compounds 5, 8, and 10 were compared with vinorelbine (VRB), vinblastine (VBL), PTX, and 2 in the OVCAR-8 and NCI/ADR-RES cell lines (Table 4). Derived from OVCAR-8, NCI/ADR-RES is a DOX-resistant cell line that overexpresses P-glycoprotein

Table 4. Growth Inhibition of OVCAR-8 and NCI/ADR-RES Cells Lines by Compounds 5, 8, and 10 and Reference Compounds VRB, VBL, PTX, and 2

compd	IC ₅₀ ± SD ^a (nM)	
	OVCAR-8 ^b	NCI/ADR-RES ^c
5	70 ± 30	25 ± 7
8	45 ± 20	25 ± 7
10	20 ± 10	15 ± 7
VRB ^d	300 ± 0	5000 ± 1000
VBL ^e	15 ± 7	200 ± 0
PTX	2 ± 0.7	1500 ± 700
2	1.3 ± 0.6	1.3 ± 0.6

^aCells were grown in RPMI 1640 medium with 5% FBS, 5% CO₂ atmosphere at 37 °C, for 96 h. ^bOVCAR-8: ovarian tumor cell line 8.

^cNCI/ADR-RES: DOX-resistant cell line derived from OVCAR-8.

^dVinorelbine, tubulin assembly inhibition = 3.1 ± 0.2 μM.

^eVinblastine, tubulin assembly inhibition = 1.1 ± 0.2 μM.

(Pgp), resulting in the type 1 multidrug-resistance phenotype. Compounds 5, 8, and 10 were uniformly more active in the NCI/ADR-RES line than in the parental OVCAR-8 line. In contrast, VRB and VBL showed the typical multidrug resistance differential, as did PTX.

CSA4 yielded the same IC₅₀ in both cell lines and clearly was not a Pgp substrate. Most importantly, as NCI/ADR-RES cell growth inhibitors, ATIs 5, 8, and 10 were all superior to VRB, VBL, and PTX. These compounds were from 200- (5 and 8) to 333-fold (10) more potent than VRB, from 13- (5 and 8) to 8-fold (10) more potent than VBL, and from 100- (5 and 8) to 60-fold (10) more potent than PTX.

Nontransformed Cell Lines. A recurrent problem with MT-targeting drugs is their widespread toxicity on normal cells when used in human patients.^{2,24,25} We therefore used nontransformed cells to evaluate potential differences between compounds 5 and 11, as representatives of one of the more potent ATIs and the least potent in the current series (Table

Table 5. Growth Inhibition of MCF-7, HOSMAC, A10, PtK2, and HUVEC Cell Lines by Compounds 2, 5, and 11 and PTX

compd	IC ₅₀ ± SD ^a (nM)				
	MCF-7	HAOSMC ^b	A10 ^c	PtK2 ^d	HUVEC ^e
5	20 ± 0	33 ± 10	40 ± 30	60 ± 0	30 ± 0
11	200 ± 0	250 ± 90	150 ± 90	300 ± 0	180 ± 40
2	13 ± 3	5 ± 3	1 ± 1	3 ± 1	1 ± 1
PTX ^f	3 ± 0.5	6 ± 6	38 ± 10	21 ± 8	7 ± 4

^aSD of 0 indicates the same value was obtained in all experiments.

^bHAOSMC: human aortic smooth muscle cells (ATCC #CLR-1999).

^cA10, rat embryonic aortic smooth muscle cells (ATCC #CRL-1476).

^dPtK2: *Potorous tridactylis* kidney epithelial cells (ATCC #CLL-56).

^eHUVEC: human umbilical vein endothelial cells (ATCC #CRL-2873). ^fData from ref 16.

5). Both compounds 5 and 11 had somewhat greater antiproliferative effects in MCF-7 breast cancer cells as compared with several nontransformed cell lines, with the difference being greater for 5 than 11. Both compounds showed less differential activity, however, than did PTX, and 2 was the least selective of the compounds evaluated.

Cell Cycle Analysis. To further characterize the cell growth inhibitory properties of the new ATIs, compounds 5

and 8–11 were analyzed for their effects on the cell cycle in parallel with VBL and 2 (Figure 1). Twenty-four hours after plating, HeLa cells were exposed to each compound for 24 h, and the cell cycle profile was subsequently analyzed by flow cytometry. We found that, for 5, 8, and 10 at 100 nM, live cell imaging (Figure 1, column A) indicates that cultures exposed to these ATIs progressed in the cell cycle up to the point where they would normally assemble the mitotic apparatus; at this point, the ATIs inhibited this assembly and prevented further progression into mitosis, inducing 70–90% of all the cells to accumulate with a G2/M DNA content (Figure 1, panels B–C), similar to VBL and 2 (80–90% G2/M arrest).

The cell cycle effects of ATIs 8 and 10 were further examined in the A549 and HT29 cell lines. Both 8 and 10 induced a gradual accumulation of cells in the G2/M phase of the cell cycle in a dose-dependent manner, and this could be detected as early as 7 h after initiation of treatment. In these cells we evaluated both the cell cycle profile and the accumulation of cyclin B1, following treatment with the compounds (Figure 2).

Mitotic Index. Both flow cytometry and the Western blot assay for cyclin B1 provide information about the entire cell population. Yet, these experiments do not provide definitive proof that the cells are actually arrested in mitosis. True arrest in mitosis would be a desirable outcome of tubulin inhibitory treatment from a therapeutic perspective, because (1), by definition, dividing cells would be selectively targeted while resting, interphase cells would be spared and (2) sustained mitotic arrest can trigger a specific cell death pathway with molecular features, such as the independence from p53, common to many tumors.²⁶ The mitotic cell death pathway can therefore operate effectively in tumor cells, including those harboring p53 mutations, differently from the classical apoptotic response induced by DNA damage that requires functional p53. To ascertain whether ATIs with cell cycle inhibitory activity induce true mitotic arrest, we processed treated cells for immunofluorescence by staining with an antibody directed against α -tubulin and with the DNA dye 4',6-diamidino-2-phenylindole (DAPI). Treated and control cells were then scored for their mitotic index (MI), calculated as mitotic cells/(mitotic + interphase cells). In control cultures, about 10% of cells were in the various stages of mitosis, with well-formed spindles interacting with condensed chromosomes (Figure 3A). In cultures exposed to ATI 5, 8, or 10, over 60% of the cells were arrested in a prometaphase-like state, with condensed chromosomes and sparse foci of tubulin that failed to elongate to form the spindle microtubules (Figure 3B). Thus, the accumulation of G2/M cells detected by flow cytometry reflected a true mitotic arrest. The MI in cell populations treated with 5, 8, and 10 was significantly higher compared with treatment with the weak tubulin inhibitor 11. The MIs observed with 5 and 10 were in the same range as with 2 and VBL, although a higher concentration of the ATIs was required (Figure 3C). Compound 9 was less effective in inducing mitotic arrest and reproducibly yielded a MI of about 35%.

Caspase-3 Expression. The data at this point indicated that most ATIs that effectively inhibited tubulin polymerization in vitro arrested mitotic progression in cultured cells, thereby causing decreased cell proliferation in human transformed cell lines. To investigate more closely the link between mitotic arrest and reduced cell growth, we analyzed HeLa cell populations exposed to 5 and 8–11 for induction of cell death under the same conditions used in the mitotic arrest

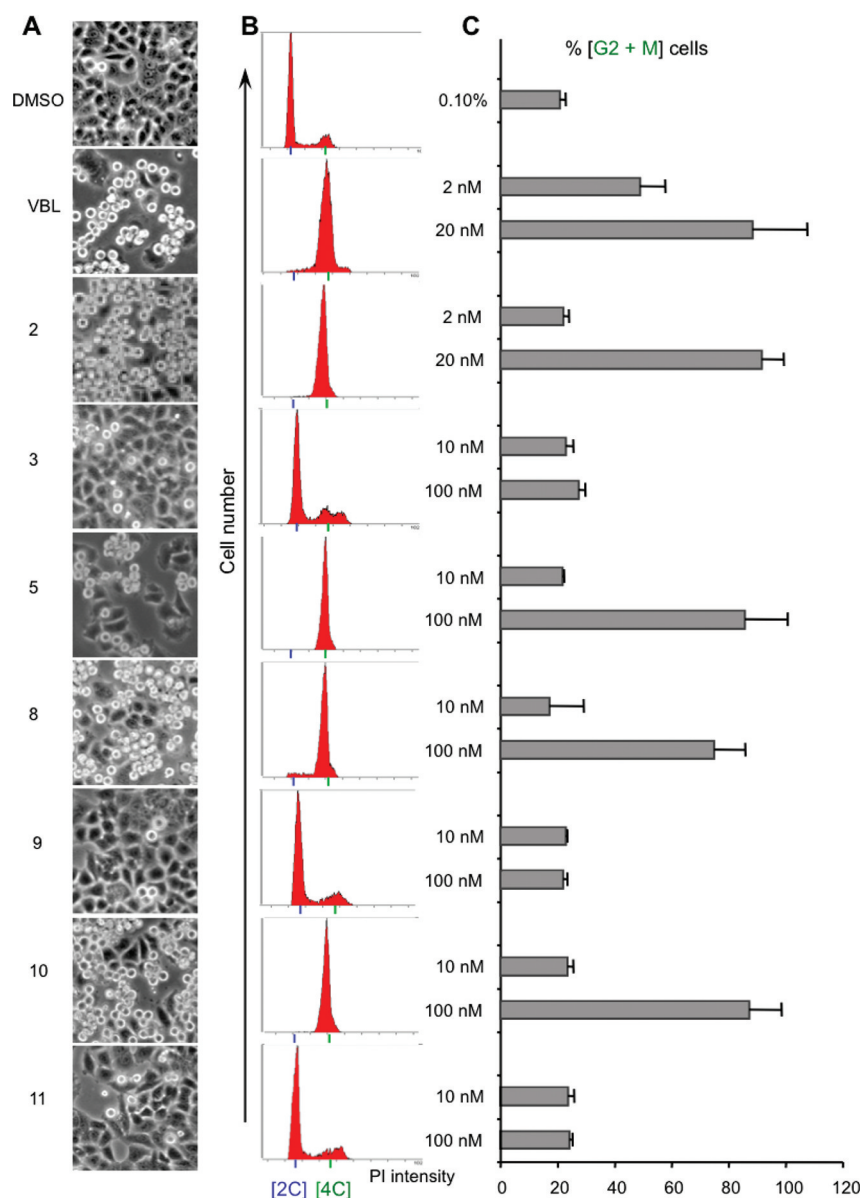


Figure 1. Effect of ATIs on HeLa cell cycle progression. (A) Bright-field panels from HeLa cell cultures exposed for 24 h to solvent (DMSO) or to the indicated compounds (VBL and 2 are shown at 20 nM; all other compounds at 100 nM). Rounded, highly refractive cells blocked in mitosis are clearly distinguishable from flattened interphase cells (10× objective). (B) Representative flow cytometry profiles of cultures exposed to compounds at the same concentrations as in part A. Cells stained with propidium iodide (PI) were separated according to their DNA content, calculated from the emitted PI fluorescence (x axis); the y axis indicates the number of cells. The 2C peak (diploid DNA content) identifies G1 cells; the 4C peak (tetraploid DNA content) identifies G2/M cells. Cells with intermediate DNA contents are in the S phase. C. Bars represent the percent of G2/M cells (4C genomic content) (mean values \pm SD were from two to six independent experiments).

experiments. Control cultures were compared with cultures treated with ATIs 5, 8, and 10 for their reactivity to annexin V, which binds to phosphatidylserine residues that are translocated from the inner to the outer cell membrane in early apoptosis. Annexin V-reactive cells were quantitated by flow cytometry (Figure 4A). The results showed that 5, 8, and 10 induced apoptosis as efficiently as 2 and VBL at the concentrations examined. To extend these results, we analyzed the induction of caspase-3 expression at the single cell level. Caspase-3 regulates the induction of apoptosis in mitotic cells, and it is required for the apoptotic response to MT-targeting drugs.^{1,27} Immunofluorescence showed that 5, 8, and 10, but not 11, induced caspase-3 activity in a significant fraction of cells (an apoptotic cell treated with 10 is shown in Figure 4B), further

demonstrating the strong link between the ability of ATIs to arrest mitotic progression and to induce apoptosis.

Metabolic Stability. An initial study with compound 3 confirmed our fears that it would be metabolically unstable, arguing against its potential as a therapeutic agent. With both mouse and human microsomal preparations, 3 was totally degraded in 30 min (Table 6). Having prepared 5, 8, and 10 and the other five-member heterocycle ATIs with the idea that they should overcome this metabolic instability, we examined these compounds in a standard microsomal stability assay (Table 6), in comparison with the control compounds 7-ethoxycoumarin and propranolol. This assay, using both human and mouse liver microsomes, estimates compound stability to phase I oxidative metabolism. Compounds 5 and 10 showed

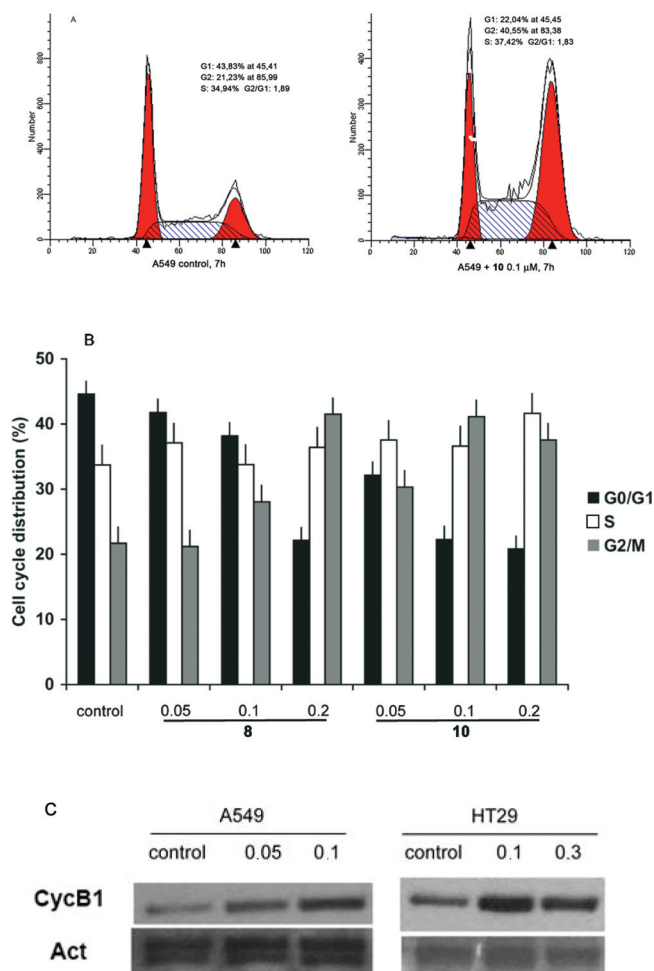


Figure 2. Dose-dependent cell cycle effects of ATI 10 in A549 and HT29 cell cultures. (A) Typical cell cycle profiles after flow cytometric analysis of A549 cell populations treated with DMSO only or with ATI 10 (100 nM, 7 h). (B) The histograms represent the percent of cells with G1, S, and G2/M DNA content, based on flow cytometric analyses of A549 cells exposed to increasing micromolar concentrations of ATIs 8 and 10 (7 h). (C) Cyclin B1 accumulation in A549 and HT29 cell lines exposed to the indicated micromolar concentrations of 10 (7 h), with actin (Act) as a loading control (Santa Cruz Biotechnology).

medium and low metabolic stability (see Table 6 legend for definitions of relative stabilities), respectively, with both the human and mouse liver microsomes, while 8 exhibited medium stability with the human microsomes and low stability with the mouse microsomes. The metabolic stability of 5, 8, and 10 may be dependent on the nature of the 2-heterocyclic nucleus rather than the structure of the bridging group. Such an effect may be explained by the steric hindrance exerted by the two aromatic moieties attached to the bridging group.

Aqueous Solubility. The aqueous solubility of 5 was 4 times greater than that of compound 3, as a result of the substitution of the pyrrole nucleus for the ester moiety. The aqueous solubility of 5 at pH 7.4 was 20 μ M, while under the same conditions the solubility of 3 was 5 μ M. This improvement in the aqueous solubility of 5 may be the explanation for the greater activity of 5 relative to 3 as an inhibitor of tubulin polymerization and MCF-7 cell growth, although the molecular modeling studies presented above suggest that 5 should bind more tightly than 3 to tubulin.

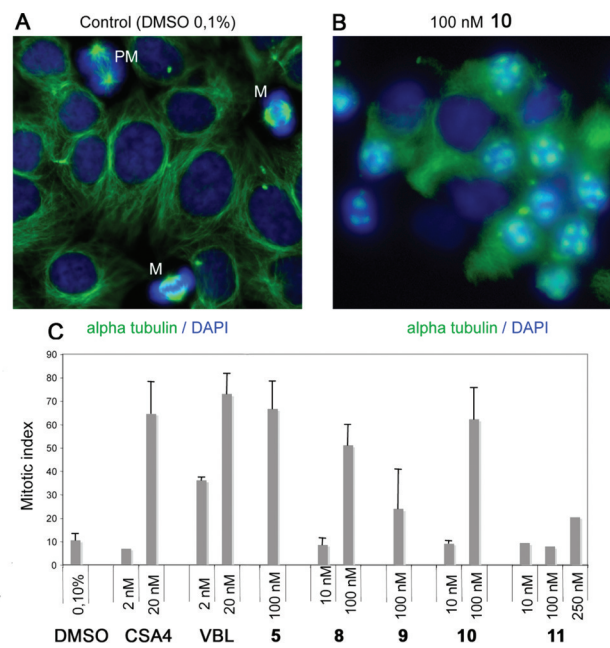


Figure 3. Induction of mitotic arrest by ATIs. (A) HeLa control cultures exposed to DMSO solvent (0.1%, 24 h). MTs were visualized by α -tubulin staining (green) and chromosomes by DNA staining (blue). Most cells were in the interphase. Cells in mitosis (PM, prometaphase; M, metaphase) are indicated. (B) A typical field from a HeLa culture exposed to ATI 10 (100 nM, 24 h). Note that most cells were arrested in early mitotic stages, with condensed chromosomes and a failure to assemble proper MTs. Disorganized tubulin foci are seen throughout the mitotic cells. (C) MIs in HeLa cell cultures that were treated with DMSO solvent, with known anti-MT compounds, or with ATIs 5 and 8–11 (mean values \pm SD were calculated from two to four independent experiments).

iv and os Pharmacokinetics. Finally, the intravenous pharmacokinetic and oral bioavailability of 5 was investigated in the mouse. Pharmacokinetic studies were carried out in male CD-1 mice. The compound was administered either in single intravenous (iv) injections of 5 mg/kg or in an oral (os) dose of 15 mg/kg. The main pharmacokinetic parameters obtained are summarized in Table 7. Compound 5 showed a systemic plasma clearance slightly lower than the hepatic blood flow of 86 mL/min·kg in mice, an estimated elimination half-life of 40 min, and a calculated steady state volume of distribution suggestive of good tissue distribution. Moreover, the compound was quickly absorbed after oral administration and showed a very high oral bioavailability. Profiles of distribution in plasma of 5 after iv and os administration and a comparison of the kinetic profiles are shown in Figures 5S and 6S, respectively, in the Supporting Information.

CONCLUSION

We designed new ATIs by replacing the 2-methoxy-/ethoxycarbonyl group (A region) with a bioisosteric 5-membered heterocycle nucleus. The newly synthesized ATIs showed effective tubulin inhibitory properties in vitro and potential therapeutic value in cancer treatment. The ATIs described here have significantly improved efficacy compared with the previously synthesized 3 used as a reference and compared well with classical MT inhibitors. In particular, the new ATIs 5, 8, and 10 showed a valuable biological profile: (i) they were potent tubulin polymerization inhibitors in the low/

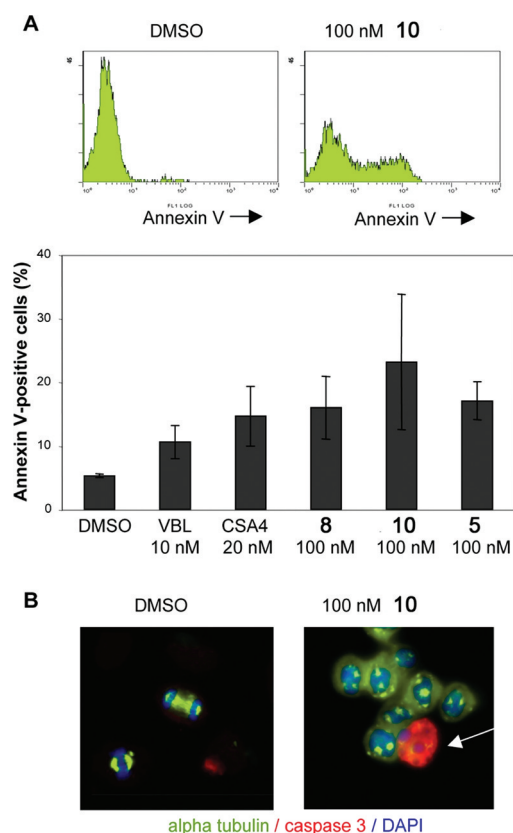


Figure 4. Induction of apoptosis by ATIs. (A) Typical flow cytometry studies of HeLa cell populations incubated with annexin V after exposure to DMSO only (control) or to **10** (100 nM). The histograms represent the percent apoptotic cells, as determined by annexin V-reactivity, after exposure to the indicated compounds for 24 h (means \pm SD were calculated from two to three experiments). (B) Single-cell level immunofluorescence analysis revealed induction of active caspase-3 (recognized by a specific antibody). The panels depict typical fields from HeLa cultures exposed to only DMSO (note the two cells progressing through mitosis) or to **10** (a mitotic cell expressing active caspase-3 is indicated by the arrow among a group of cells arrested in mitosis).

Table 6. Metabolic Stability of 5, 8, and 10 with Human and Mouse Liver Microsomes^a

compd	% remaining at 30 min ^b	
	human liver microsomes	mouse liver microsomes
5	34.8 \pm 1.4	23.1 \pm 0.6
8	22.0 \pm 1.0	2.2 \pm 0.3
10	4.6 \pm 0.2	0.60 \pm 0.01
3	0.37 \pm 0.01	0.5 \pm 0.03
7-ethoxycoumarin ^c	6.6 \pm 0.2	0.07 \pm 0.02
propranolol ^c	54.1 \pm 0.4	20.6 \pm 0.5

^aMetabolic stability: >95, high; 50–95, good; 10–50, medium; <10, low. ^bResults are expressed as mean \pm SD, $n = 2$. ^cThe standard compounds 7-ethoxycoumarin and propranolol showed metabolic stability in agreement with the literature and internal validation data.²⁸

submicromolar range of concentration; (ii) such compounds were uniformly more active in the Pgp-overexpressing NCI/ADR-RES cell line than in the parental OVCAR-8 line and were superior to VRB, VBL, and PTX; (iii) compounds **5** and **10** showed selective activity against cells with acquired cisplatin resistance; (iv) they reduced cell growth in a panel of human

Table 7. Pharmacokinetic Properties of 5 in Mice

parameter	value
C_{\max}^a (iv) (ng/mL)	35.67
$AUC_{0-\infty}^b$ (iv) (ng-min/mL)	174346
$t_{1/2}^c$ (min)	40
Cl^d (mL/min-kg)	28.6
V_{ss}^e (L/kg)	1.59
C_{\max}^a (os) (ng/mL)	1340
t_{\max}^f (os) (min)	120
$AUC_{0-\infty}^b$ (os) (ng-min/mL)	583315
F^g (%)	110

^aMaximum concentration. ^bArea under the curve calculated up to the 0– ∞ time point. ^cHalf-time. ^dClearance. ^eMean distribution volume. ^fmax-time. ^gOral bioavailability.

transformed cell lines *via* arrest of mitotic progression and induction of cell death; (v) the induction of mitotic arrest in cell populations treated with these ATIs was in the same range as was observed with CSA4 and VBL; (vi) they induced apoptosis in the same range or above the level induced by VBL and CSA4 and triggered caspase-3 activation; (vii) the sulfur bridging group of ATIs showed satisfactory metabolic stability. We would like to highlight their effectiveness in the HeLa and 231-MDA cell lines, both of which lack functional p53: this indicates that the cell death pathway triggered by ATIs is p53-independent. This is of relevance from a therapeutic perspective, given that about 50% of all human tumors are defective for p53 function and cannot respond to DNA-targeting drugs, which induce p53-dependent apoptosis. On the whole, the present data strongly support the therapeutic potential and further development of the new ATIs described here. Finally, the metabolic stability of compound **5**, obtained in both mouse and human microsomes, along with the excellent mouse pharmacokinetic profile, warrant further *in vivo* efficacy studies.

EXPERIMENTAL SECTION

Chemistry. MW-assisted reactions were performed on a Discover S-Class (CEM) single mode reactor, controlling instrument parameters with PC-running Synergy 1.4 software. Temperature, irradiation power, maximum pressure (Pmax), PowerMAX (in situ cooling during the MW irradiation), ramp and hold times, and open and closed vessel modes were set as indicated. Reactions in an open vessel were carried out in 100 mL round-bottom flasks equipped with a Dimroth reflux condenser and a cylindrical stirring bar (length 20 mm, diameter 6 mm). Reactions in a closed vessel were performed in capped MW-dedicated vials (10 mL) with a cylindrical stirring bar (length 8 mm, diameter 3 mm). The temperature of the reaction was monitored with a built-in infrared (IR) sensor. After completion of the reaction, the mixture was cooled to 25 °C via air-jet cooling. Melting points (mp's) were determined on a SMP1 apparatus (Stuart Scientific) and are uncorrected. IR spectra were run on a SpectrumOne FT-ATR spectrophotometer (Perkin-Elmer). Band position and absorption ranges are given in inverse centimeters. Proton nuclear magnetic resonance (¹H NMR) spectra were recorded on a 400 MHz FT spectrometer (Bruker) in the indicated solvent. Chemical shifts are expressed in δ units (ppm) from tetramethylsilane. Mass spectra were recorded on a Bruker MicroTOF LC column. Column chromatography was performed on columns packed with alumina from Merck (70–230 mesh) or silica gel from Macherey-Nagel (70–230 mesh). Aluminum oxide thin layer chromatography (TLC) cards from Fluka (aluminum oxide precoated aluminum cards with fluorescent indicator visualizable at 254 nm) and silica gel TLC cards from Macherey-Nagel (silica gel precoated aluminum cards with fluorescent indicator visualizable at 254 nm) were used for TLC.

Developed plates were visualized with a Spectroline ENF 260C/FE UV apparatus. Organic solutions were dried over anhydrous sodium sulfate. Evaporation of the solvents was carried out on a Büchi Rotavapor R-210 equipped with a Büchi V-850 vacuum controller and Büchi V-700 and V-710 vacuum pumps. Elemental analyses of the new compounds were found within 0.4% of the theoretical values. The purity of tested compounds was >95%. Compounds **20**, **22**, **25**, and **27** were purchased from Sigma-Aldrich.

General Procedure for the Preparation of Compounds 4–8 and 12. Example. 2-(1*H*-Pyrrol-2-yl)-3-[(3',4',5'-trimethoxyphenyl)thio]-1*H*-indole (4). 2-(1*H*-Pyrrol-2-yl)-1*H*-indole¹⁹ (**13**) (0.25 g, 0.0014 mol) was carefully added to a suspension of sodium hydride (60% in mineral oil, 0.13 g, 0.0031 mol) in anhydrous DMF (2 mL) while stirring. After 10 min, bis(3,4,5-trimethoxyphenyl)disulfide¹³ (0.62 g, 0.0015 mol) was added, and the reaction mixture was placed into the MW cavity (closed vessel mode, Pmax = 250 PSI). MW irradiation of 150 W was used, the temperature being ramped from 25 to 110 °C while stirring. Once 110 °C was reached, taking about 1 min, the reaction mixture was held there for 2 min. The mixture was diluted with water and extracted with ethyl acetate. The organic layer was washed with brine and dried. Removal of the solvent gave a residue that was purified by column chromatography (alumina, chloroform as eluent) to furnish **4** (0.1 g, 19%), mp 215–218 °C (from ethanol). ¹H NMR (DMSO-*d*₆): δ 3.52 (s, 6H), 3.55 (s, 3H), 6.18 (t, *J* = 2.9 Hz, 1H), 6.34 (s, 2H), 6.81 (d, *J* = 2.4 Hz, 1H), 6.96 (br s, 1H), 7.04–7.08 (m, 1H), 7.12–7.16 (m, 1H), 7.42 (d, *J* = 8.1 Hz, 2H), 11.11 (br s, 1H, disappeared on treatment with D₂O), 11.64 ppm (br s, 1H, disappeared on treatment with D₂O). MS: ES⁺ = 381 (MH⁺). IR: ν 3329, 3422 cm⁻¹. Anal. (C₂₁H₂₀N₂O₃S (380.46)) C, H, N, S.

2-(1*H*-Pyrrol-3-yl)-3-[(3',4',5'-trimethoxyphenyl)thio]-1*H*-indole (5). Synthesized as **4**, starting from **14**, yield 10% as a brown solid, mp 200–204 °C (from ethanol). ¹H NMR (DMSO-*d*₆): δ 3.52 (s, 6H), 3.56 (s, 3H), 6.33 (s, 2H), 6.75–6.77 (m, 1H), 6.84–6.86 (m, 1H), 7.00–7.04 (m, 1H), 7.08–7.12 (m, 1H), 7.39 (d, *J* = 8.6 Hz, 2H), 7.48–7.50 (m, 1H), 11.11 (br s, 1H, disappeared on treatment with D₂O), 11.58 ppm (br s, 1H, disappeared on treatment with D₂O). MS: ES⁺ = 381 (MH⁺). IR: ν 3358, 3390 cm⁻¹. Anal. (C₂₁H₂₀N₂O₃S (380.46)) C, H, N, S.

2-(Furan-2-yl)-3-[(3',4',5'-trimethoxyphenyl)thio]-1*H*-indole (6). Synthesized as **4**, starting from **15**, yield 38% as a white solid, mp 180–184 °C (from ethanol). ¹H NMR (CDCl₃): δ 3.65 (s, 6H), 3.77 (s, 3H), 6.38 (s, 2H), 6.54 (q, *J* = 1.8 Hz, 1H), 7.17–7.20 (m, 1H), 7.24–7.25 (m, 2H), 7.44 (d, *J* = 8 Hz, 1H), 7.50 (m, 1H), 7.67 (d, *J* = 8 Hz, 1H), 8.94 ppm (br s, 1H, disappeared on treatment with D₂O). MS: ES⁺ = 382 (MH⁺). IR: ν 3333 cm⁻¹. Anal. (C₂₁H₁₉NO₄S (381.44)) C, H, N, S.

2-(Furan-3-yl)-3-[(3',4',5'-trimethoxyphenyl)thio]-1*H*-indole (7). Synthesized as **4**, starting from **16**, yield 42% as a brown solid, mp 185–190 °C (from ethanol). ¹H NMR (DMSO-*d*₆): δ 3.64 (s, 6H), 3.76 (s, 3H), 6.34 (s, 2H), 6.87 (m, 1H), 7.16 (t, *J* = 7.5 Hz, 1H), 7.22–7.26 (m, 1H), 7.41 (d, *J* = 8.0 Hz, 1H), 7.51 (t, *J* = 1.6 Hz, 1H), 7.65 (dd, *J* = 0.6 and 7.8 Hz, 1H), 8.08–8.09 (m, 1H), 8.50 ppm (br s, 1H, disappeared on treatment with D₂O). MS: ES⁺ = 382 (MH⁺). IR: ν 3330 cm⁻¹. Anal. (C₂₁H₁₉NO₄S (381.44)) C, H, N, S.

2-(Thiophen-2-yl)-3-[(3',4',5'-trimethoxyphenyl)thio]-1*H*-indole (8). Synthesized as **4**, starting from **17**, yield 60% as a yellow solid, mp 195–198 °C (from ethanol). ¹H NMR (DMSO-*d*₆): δ 3.53 (s, 6H), 3.56 (s, 3H), 6.35 (s, 2H), 7.09–7.13 (m, 1H), 7.19–7.24 (m, 2H), 7.47–7.49 (m, 2H), 7.65 (dd, *J* = 1.1 and 5.0 Hz, 1H), 7.77 (dd, *J* = 1.1 and 3.7 Hz, 1H), 12.11 ppm (br s, 1H, disappeared on treatment with D₂O). MS: ES⁺ = 398 (MH⁺). IR: ν 3317 cm⁻¹. Anal. (C₂₁H₁₉NO₃S₂ (397.51)) C, H, N, S.

2-(Thiophen-3-yl)-3-[(3',4',5'-trimethoxyphenyl)thio]-1*H*-indole (12). Synthesized as **4**, starting from **19**, yield 83% as a white solid, mp 220–225 °C (from ethanol). ¹H NMR (CDCl₃): δ 3.64 (s, 6H), 3.78 (s, 3H), 6.37 (s, 2H), 7.17–7.21 (m, 1H), 7.25–7.29 (m, 1H), 7.42–7.44 (m, 2H), 7.64 (dd, *J* = 1.3 and 5.0 Hz, 1H), 7.68 (d, *J* = 7.8 Hz, 1H), 7.85 (dd, *J* = 1.3 and 3.0 Hz, 1H), 8.62 ppm (br s, 1H, disappeared on treatment with D₂O). MS: ES⁺ = 398 (MH⁺). IR: ν 3331 cm⁻¹. Anal. (C₂₁H₁₉NO₃S₂ (397.51)) C, H, N, S.

5-Methoxy-2-(thiophen-2-yl)-3-[(3',4',5'-trimethoxyphenyl)thio]-1*H*-indole (9). **18** (0.19 g, 0.00083 mol) was added at 0 °C to a suspension of sodium hydride (60% in mineral oil, 0.05 g, 0.0012 mol) in anhydrous DMF (2 mL). After 15 min, bis(3,4,5-trimethoxyphenyl)disulfide¹⁴ (0.36 g, 0.00091 mol) was added, and the reaction was heated at 110 °C overnight under an Ar stream. After cooling, the mixture was carefully diluted with water and extracted with ethyl acetate. The organic layer was washed with brine and dried. Removal of the solvent gave a residue that was purified by column chromatography (silica gel, ethyl acetate/*n*-hexane 1:2 as eluent) to furnish **9** as a white solid (0.25 g, 70%), mp 55–58 °C (from ethanol). ¹H NMR (CDCl₃): δ 3.67 (s, 6H), 3.78 (s, 3H), 3.84 (s, 3H), 6.39 (s, 2H), 6.92 (dd, *J* = 2.5 and 8.7 Hz, 1H), 7.11–7.13 (m, 2H), 7.31 (dd, *J* = 0.5 and 8.7 Hz, 1H), 7.39 (dd, *J* = 1.1 and 5.1 Hz, 1H), 7.52 (dd, *J* = 1.1 and 3.7 Hz, 1H), 8.54 ppm (br s, 1H, disappeared on treatment with D₂O). MS: ES⁺ = 428 (MH⁺). IR: ν 3301 cm⁻¹. Anal. (C₂₂H₂₁NO₄S₂ (427.54)) C, H, N, S.

[2-(Thiophen-2-yl)-1*H*-indol-3-yl]-(3',4',5'-trimethoxyphenyl)methanone (10). A mixture of **17** (0.25 g, 0.00125 mol), 3,4,5-trimethoxybenzoyl chloride (0.29 g, 0.00125 mol), and anhydrous aluminum chloride (0.17 g, 0.00125 mol) in anhydrous 1,2-dichloroethane (2 mL) was placed into the MW cavity (closed vessel mode, Pmax = 250 PSI). MW irradiation of 150 W was used, the temperature being ramped from 25 to 110 °C with stirring. Once 110 °C was reached, taking about 1 min, the reaction mixture was held there for 2 min. The reaction mixture was quenched on 1 N HCl/crushed ice and extracted with chloroform. The organic layer was washed with brine and dried. Removal of the solvent gave a residue that was purified by column chromatography (silica gel, ethyl acetate/*n*-hexane 3:7 as eluent) to furnish **10** as a yellow solid (0.17 g, 34%), mp 155–159 °C (from ethanol). ¹H NMR (DMSO-*d*₆): δ 3.75 (s, 6H), 3.88 (s, 3H), 6.96–6.98 (m, 1H), 7.08 (s, 2H), 7.20–7.24 (m, 2H), 7.30–7.34 (m, 2H), 7.45 (d, *J* = 8.0 Hz, 1H), 7.80 (d, *J* = 7.8 Hz, 1H), 8.73 ppm (br s, 1H, disappeared on treatment with D₂O). MS: ES⁺ = 394 (MH⁺). IR: ν 1570, 3214 cm⁻¹. Anal. (C₂₂H₁₉NO₄S (393.46)) C, H, N, S.

2-(Thiophen-2-yl)-3-(3',4',5'-trimethoxybenzyl)-1*H*-indole (11). A mixture of **10** (0.1 g, 0.00025 mol) and sodium borohydride (0.1 g, 0.0025 mol) in ethanol (10 mL) was heated to reflux for 2.5 h. After cooling, the reaction mixture was diluted with water and extracted with ethyl acetate. The organic layer was washed with brine and dried. Removal of the solvent gave a residue that was purified by column chromatography (silica gel, ethyl acetate/*n*-hexane 3:7 as eluent) to furnish **11** as a brown solid (0.02 g, 21%), mp 43–47 °C (from ethanol). ¹H NMR (CDCl₃): δ 3.73 (s, 6H), 3.80 (s, 3H), 4.27 (s, 2H), 6.47 (s, 2H), 7.07–7.13 (m, 2H), 7.19–7.23 (m, 2H), 7.35–7.39 (m, 2H), 7.49 (d, *J* = 7.9 Hz, 1H), 8.17 ppm (br s, 1H, disappeared on treatment with D₂O). MS: ES⁺ = 380 (MH⁺). IR: ν 3340 cm⁻¹. Anal. (C₂₂H₂₁NO₃S (379.47)) C, H, N, S.

2-(2-Nitrophenyl)-1-[1-(phenylsulfonyl)-1*H*-pyrrol-3-yl]-ethan-1-one (21). Oxalyl chloride (2.46 g, 1.64 mL, 0.019 mol) and a catalytic amount of anhydrous DMF were added at 0 °C to **20** (3.52 g, 0.019 mol) in anhydrous 1,2-dichloroethane (88 mL) under an Ar stream. After 30 min, 1-(phenylsulfonyl)-1*H*-pyrrole (4.04 g, 0.0019 mol) and anhydrous aluminum chloride (2.59 g, 0.0019 mol) were added. The reaction mixture was stirred at 0 °C for 25 min, quenched on 1 N HCl/crushed ice, and extracted with chloroform. The organic layer was washed with brine and dried. Removal of the solvent gave a residue that was purified by column chromatography (silica gel, acetone/*n*-hexane 1:2 as eluent) to furnish **21** as a yellow solid (0.7 g, 10%), mp 135 °C (from ethanol). ¹H NMR (DMSO-*d*₆): δ 4.45 (s, 2H), 6.41–6.43 (m, 1H), 7.25–7.30 (m, 2H), 7.45–7.60 (m, 5H), 7.85–7.86 (m, 1H), 7.90–7.92 (m, 2H), 8.06 ppm (dd, *J* = 1.2 and 8.2 Hz, 1H). IR: ν 1680 cm⁻¹. Anal. (C₁₈H₁₄N₂O₅S (370.38)) C, H, N, S.

2-[1-(Phenylsulfonyl)-1*H*-pyrrol-3-yl]-1*H*-indole (14). A mixture of **21** (0.25 g, 0.0007 mol) and iron powder (0.27 g, 0.0049 mol) in glacial acetic acid (8 mL) was heated at 60 °C overnight. After cooling, the mixture was diluted with water while stirring and extracted with ethyl acetate. The organic layer was washed with brine and dried. Removal of the solvent gave a residue that was purified by column

chromatography (silica gel, ethyl acetate/*n*-hexane 1:3 as eluent) to furnish **14** as a white solid (0.7 g, 10%), mp 180–185 °C (from ethanol). ¹H NMR (DMSO-*d*₆): δ 6.66 (d, *J* = 1.4 Hz, 1H), 6.83–6.85 (m, 1H), 6.93–6.97 (m, 1H), 7.02–7.07 (m, 1H), 7.31 (d, *J* = 8.0 Hz, 1H), 7.44–7.46 (m, 2H), 7.65–7.69 (m, 2H), 7.74–7.79 (m, 1H), 7.84 (t, *J* = 1.9 Hz, 1H), 7.98–8.00 (m, 2H), 11.30 ppm (br s, 1H, disappeared on treatment with D₂O). IR: ν 3407 cm⁻¹. Anal. (C₁₈H₁₄N₂O₂S (322.38)) C, H, N, S.

1-(1-(Furan-2-yl)ethylidene)-2-phenylhydrazine (23). A mixture of phenylhydrazine hydrochloride (3.91 g, 0.027 mol), **22** (2.0 g, 1.82 mL, 0.018 mol), and anhydrous sodium acetate (2.21 g, 0.027 mol) in ethanol (25 mL) was placed into the microwave cavity (open vessel mode). Microwave irradiation of 250 W was used, the temperature being ramped from 25 to 80 °C. Once 80 °C was reached, taking about 1 min, the reaction mixture was held there for 5 min, while stirring and cooling. The reaction mixture was filtered to give **23** as an orange solid (2.9 g, 96%), mp 79–84 °C (from ethanol). ¹H NMR (DMSO-*d*₆): δ 2.19 (s, 3H), 6.54–6.55 (m, 1H), 6.70–6.71 (m, 1H), 6.74–6.77 (m, 1H), 7.18–7.23 (m, 4H), 7.68–7.69 (m, 1H), 9.22 ppm (broad s, disappeared on treatment with D₂O, 1H). IR: ν 3342 cm⁻¹. Anal. (C₁₂H₁₂N₂O₂ (200.24)) C, H, N.

2-(Furan-2-yl)-1H-indole (15). **23** (1.18 g, 0.006 mol) was added portionwise to PPA (10 g) preheated at 110 °C, and the reaction mixture was stirred at the same temperature for 1 h. After quenching on crushed ice, the mixture was stirred at 25 °C overnight; then it was made basic (pH = 10) with a saturated solution of potassium carbonate and extracted with ethyl acetate. The organic layer was washed with brine and dried. Removal of the solvent gave a residue that was purified by column chromatography (alumina, ethyl acetate/*n*-hexane 1:5 as eluent) to furnish **15** as a yellow solid (0.6 g, 55%), mp 123–125 °C (from ethanol). Lit.²⁹ 120–123 °C.

2-(Furan-3-yl)-1H-indole (16). A mixture of 2-iodo-1H-indole²⁹ (0.25 g, 0.001 mol), furan-3-boronic acid pinacol ester (0.26 g, 0.00134 mol), potassium carbonate (0.18 g, 0.00134 mol), and Pd(II) acetate (0.03 g, 0.000134 mol) in 1-methyl-2-pyrrolidinone (2.3 mL) containing 0.18 mL of water was degassed for 15 min and placed into the MW cavity (closed vessel mode, Pmax = 250 psi). MW irradiation of 200 W was used, the temperature being ramped from 25 to 110 °C while stirring. Once 110 °C was reached, taking about 2 min, the reaction mixture was held there for 15 min. After cooling, the mixture was diluted with water and extracted with ethyl acetate. The organic layer was washed with brine and dried. Removal of the solvent gave a residue that was purified by column chromatography (silica gel, ethyl acetate/*n*-hexane 1:5 as eluent) to furnish **16** as a white solid (0.18 g, 95%), mp 145–148 °C (from ethanol). ¹H NMR (CDCl₃): δ 6.61–6.62 (m, 1H), 6.70–6.71 (m, 1H), 7.09–7.19 (m, 2H), 7.36 (dd, *J* = 0.9 and 8.0 Hz, 1H), 7.50–7.52 (m, 1H), 7.58–7.60 (m, 1H), 7.75 (m, 1H), 8.10 ppm (broad s, disappeared on treatment with D₂O, 1H). IR: ν 3417 cm⁻¹. Anal. (C₁₂H₉NO (183.21)) C, H, N.

2-Bromo-1-(thiophen-2-yl)ethan-1-one (26). A solution of bromine (2.53 g, 0.82 mL, 0.0158 mol) in dichloromethane (8 mL) was added dropwise to **25** (2.0 g, 1.71 mL, 0.0158 mol) in the same solvent (10 mL). The reaction mixture was stirred at 25 °C for 1 h and neutralized with a saturated solution of sodium hydrogen carbonate. The organic layer was washed with brine and dried. Removal of the solvent gave a residue that was purified by column chromatography (silica gel, ethyl acetate/*n*-hexane 5:95 as eluent) to furnish **26** as a yellow oil (2.60 g, 80%).³⁰

2-(Thiophen-2-yl)-1H-indole (17). A mixture of **26** (0.5 g, 0.0024 mol) and aniline (0.4 g, 0.4 mL, 0.0041 mol) was kept at 25 °C for 3 h with occasional stirring; then a catalytic amount of anhydrous DMF was added, and the reaction mixture was placed into the MW cavity (closed vessel mode, Pmax = 250 PSI). MW irradiation of 150 W was used, the temperature being ramped from 25 to 100 °C while stirring. Once 100 °C was reached, taking about 1 min, the reaction mixture was held there for 1 min. The mixture was diluted with 1 N HCl and extracted with ethyl acetate. The organic layer was washed with brine and dried. Removal of the solvent gave a residue that was purified by column chromatography (silica gel, ethyl acetate/*n*-hexane

3:7 as eluent) to furnish **17** as a yellow solid (0.19 g, 40%), mp 175–180 °C (from cyclohexane). Lit.³¹ 167–168 °C (from hexane).

2-Bromo-1-(thiophen-3-yl)ethanone (28). Synthesized as **26**, starting from **27**. Yield 57% as a brown solid, mp 60–65 °C (from ethanol). ¹H NMR (CDCl₃): δ 4.34 (s, 2H), 7.35–7.37 (m, 1H), 7.57 (dd, *J* = 1.3 and 5.1 Hz, 1H), 8.17–8.18 ppm (m, 1H). IR: ν 1672 cm⁻¹. Anal. (C₆H₅BrOS (205.07)) C, H, Br, S.

2-(Thiophen-3-yl)-1H-indole (19). Synthesized as **17**, starting from **28**. Yield 16% as a yellow solid, mp 210–215 °C (from cyclohexane). Lit.³² 212–214 °C.

2-(5-Methoxy-2-nitrophenyl)-1-(thiophen-2-yl)ethanol (30). TBAF (1 M in THF, 0.83 mL, 0.00083 mol) was dropped into a solution of **29**²⁶ (0.2 g, 0.00083 mol) and thiophen-2-carboxaldehyde (0.11 g, 0.092 mL, 0.001 mol) in anhydrous THF (5 mL) at 25 °C under an Ar stream. After 15 min, 37% HCl (0.83 mL) was added, and the reaction mixture was extracted with diethyl ether, washed with brine, and dried. Removal of the solvent gave a residue that was purified by column chromatography (silica gel, chloroform as eluent) to furnish **30** as a yellow oil (0.14 g, 61%). ¹H NMR (CDCl₃): δ 2.46 (d, *J* = 4.2 Hz, 1H), 3.37 (dd, *J* = 8.4 and 13.3 Hz, 1H), 3.55 (dd, *J* = 4.4 and 13.3 Hz, 1H), 3.84 (s, 3H), 5.31–5.35 (m, 1H), 6.77 (d, *J* = 2.8 Hz, 1H), 6.86 (dd, *J* = 2.8 and 9.1 Hz, 1H), 6.97–7.02 (m, 2H), 7.27–7.30 (m, 1H), 8.08 ppm (d, *J* = 9.1 Hz, 1H). IR: ν 3289 cm⁻¹. Anal. (C₁₃H₁₃NO₄S (279.31)) C, H, N, S.

2-(5-Methoxy-2-nitrophenyl)-1-(thiophen-2-yl)ethan-1-one (31). A solution of **30** (0.74 g, 0.00265 mol) in anhydrous dichloromethane (1.7 mL) was dropped into a suspension of pyridium chlorochromate (0.87 g, 0.004 mol) in the same solvent (6 mL). The reaction mixture was stirred at 25 °C for 1.5 h and filtered. After removal of the solvent, the crude product was purified by column chromatography (silica gel, chloroform as eluent) to furnish **31** as a white solid (0.7 g, 56%), mp 140–145 °C (from ethanol). ¹H NMR (CDCl₃): δ 3.90 (s, 3H), 4.65 (s, 2H), 6.83 (d, *J* = 2.7 Hz, 1H), 6.93 (dd, *J* = 2.8 and 9.1 Hz, 1H), 7.14–7.20 (m, 1H), 7.65–7.69 (m, 1H), 7.84–7.92 (m, 1H), 8.22 ppm (d, *J* = 9.2 Hz, 1H). IR: ν 1654 cm⁻¹. Anal. (C₁₃H₁₁NO₄S (277.30)) C, H, N, S.

5-Methoxy-2-(thiophen-2-yl)-1H-indole (18). A mixture of **30** (1.07 g, 0.0039 mol) and tin(II) chloride dihydrate (4.98 g, 0.019 mol) in ethyl acetate was heated to reflux for 3 h. After cooling, the reaction mixture was made basic (pH = 10) with a saturated potassium carbonate solution. The suspension was filtered and the layers were separated. The organic layer was washed with brine and dried. Removal of the solvent gave a residue that was purified by column chromatography (silica gel, dichloromethane as eluent) to furnish **18** as a yellow solid (0.19 g, 21%), mp 125 °C (from ethanol). Lit.³³ 124 °C.

Biology. Tubulin Assembly. The reaction mixtures contained 0.8 M monosodium glutamate (pH 6.6 with HCl in a 2 M stock solution), 10 μM tubulin, and varying concentrations of compound. Following a 15 min preincubation at 30 °C, samples were chilled on ice, GTP to 0.4 mM was added, and turbidity development was followed at 350 nm in a temperature controlled recording spectrophotometer for 20 min at 30 °C. Extent of reaction was measured. Full experimental details were previously reported.³⁴

[³H]Colchicine Binding Assay. The reaction mixtures contained 1.0 μM tubulin, 5.0 μM [³H]colchicine, and 5.0 μM inhibitor and were incubated for 10 min at 37 °C. Complete details were described previously.³⁵

Cell Cultures and Treatment. Cell lines were obtained from the American Tissue Culture Collection (ATCC), unless specified otherwise. Cells were grown in Dulbecco's Modified Eagle medium (D-MEM) supplemented with 10% fetal bovine serum (FBS) at 37 °C with 5% CO₂. In all experiments 300,000 cells were plated in 9 cm² dishes and exposed to test compound dissolved in DMSO (0.1% final concentration) at the indicated concentrations.

The methodology for the evaluation of the growth of human MCF-7 breast carcinoma, OVCAR-8, and NCI/ADR-RES cells, obtained from the National Cancer Institute drug screening laboratory, was previously described, except that cells were grown for 96 h for IC₅₀ determinations.⁴⁶ HeLa, PC3, HT29, and A549 cell lines were grown

at 37 °C in D-MEM containing 10 mM glucose supplemented with 10% FBS, 100 units/mL each of penicillin and streptomycin, and 2 mM glutamine. At the onset of each experiment, cells were placed in fresh medium and cultured in the presence of test compounds from 0.01 to 25 μ M. 231-MDA and A549 cells were cultured in DMEM supplemented with 10% FBS for 24, 48, and 72 h in a 96-well tissue culture plate at 37 °C and 5% CO₂ in the absence or presence of different drug concentrations.

The *Potorus tridactylis* PtK2 cells, the A10 rat embryonic aortic smooth muscle cells, the human umbilical vein endothelial cells, and the human aortic smooth muscle cells were obtained from ATCC and grown as recommended, except that a 5% CO₂ atmosphere was used with all cells.

Evaluation of growth inhibition of the A2780wt, A2780-CIS, and OVCAR-3 cell lines was performed as previously reported.³⁶

Cell Viability Assay. Cell viability was generally determined using the MTT colorimetric assay. The test is based on the ability of mitochondrial dehydrogenase to convert, in viable cells, the yellow MTT reagent into a soluble blue formazan dye. Cells were seeded into 96-well plates to a density of $7 \times 10^3/100 \mu\text{L}$ well. After 24 h of growth to allow attachment to the wells, compounds were added at various concentrations (from 0.01 to 25 μ M). After 48 h of growth and removal of the culture medium, 100 μL /well of medium containing 1 mg/mL of MTT was added. Cell cultures were further incubated at 37 °C for 2 h in the dark. The solution was then gently aspirated from each well, and the formazan crystals within the cells were dissolved with 100 μL of DMSO. Optical densities were read at 550 nm using a Multiskan Spectrum Thermo Electron Corporation reader. Results were expressed as percentage relative to vehicle-treated control (0.5% DMSO was added to untreated cells), and IC₅₀ values were determined by linear and polynomial regression. Experiments were performed in triplicate.

231-MDA and A549 cells were plated at different cellular densities in order to test the compounds on logarithmic phase cells. Test compounds were added after cell adhesion. On the day of the assay, 10 μL MTT (5 mg/mL) was added to each well, and cells were incubated for 2 h (37 °C, 5% CO₂). When dark crystals appeared at the well bottom, culture medium was discarded, and ethanol (100 μL) was added to each well to solubilize the crystals, yielding a purple solution. Absorbance was read with an enzyme-linked immunosorbent assay (ELISA) reader at 570 nm.

Immunofluorescence Assay. Cells to be processed for immunofluorescence were grown on sterile poly-L-lysine (SIAL) coated coverslips. After treatment, cells were either simultaneously fixed and permeabilized in MeOH for 6 min at -20 °C or, alternatively, first fixed in 3.7% paraformaldehyde (PFA) for 10 min followed by permeabilization in 0.1% Triton-X 100. The following antibodies were used: anti- β -tubulin unconjugated (Sigma clone B5.1.2, 1:2000) or FITC-conjugated (Sigma, 1:150); anti- γ -tubulin (Sigma, 1:1000); antiprocessed caspase-3 (Cell Signaling Technology, 9661, 1:500). Antibodies attached to their antigens were detected using secondary antibodies: antimouse Texas Red (Vector, TI-2000, 1:800), antimouse FITC (Jackson ImmunoResearch Laboratories, 115-095-068, 1:200), antimouse AMCA (1:50), antirabbit FITC (Santa Cruz, sc-2090, 1:100), antirabbit Cy3 (Jackson ImmunoResearch Laboratories, 711-165-152, 1:1000). The DNA was stained with DAPI (Sigma, 0.05 $\mu\text{g}/\text{mL}$ in H₂O). Slides were finally mounted in Vectashield (Vector).

Microscopy. Bright-field images of growing cells were taken under an inverted fluorescence microscope (Nikon TE 300) equipped with a DMX1200-type CCD (resolution 1280 pixels \times 1024), using ACT-1 software. Immunofluorescence images were obtained under an epifluorescence Olympus AX70 microscope equipped with a CCD camera (Diagnostic Instruments, Spot RT slider model 2.3.0) or a Nikon Eclipse 90i microscope equipped with Qimaging camera and the NisElements AR 3.1 software (Nikon).

Flow Cytometry. Cell cycle distribution was analyzed after cell incubation with propidium iodide (Sigma). Apoptosis was analyzed after incubation of cells with annexin V-FITC (Immunofluorescence Science). Cell samples were analyzed in a Coulter Epics XL

cytofluorometer (Beckman Coulter) equipped with EXPO 32 ADC software. Data for at least 10000 cells per sample were acquired.

Western Blotting Analysis. Cells were plated in flasks (1×10^6 cells) and incubated with or without an ATI compound. At the indicated times, cells were lysed using ice cold lysis buffer (50 mM Tris, 150 mM NaCl, 10 mM EDTA, 1% Triton) supplemented with protease inhibitor cocktail (antipain, bestatin, chymostatin, leupeptin, pepstatin, phosphoramidon, Pefabloc, EDTA, and aprotinin, all from Boehringer). Whole cell extracts were loaded on 8–12% sodium dodecyl sulfate polyacrylamide gels and electrophoresed, followed by blotting onto nitrocellulose membranes (BioRad). After membrane blocking with 5% (w/v) fat-free milk powder, 0.1% Tween 20 in Tris buffered saline (TBS), the membrane was incubated overnight at 4 °C with specific antibodies at the concentrations indicated by the manufacturers (Cell Signaling Technology and Santa Cruz Biotechnology) in Tris-buffered saline/Tween-20/5% milk. Following incubation with horseradish peroxidase-conjugated secondary antibody, bands were detected by enhanced chemiluminescence (ECL kit, Amersham). Each filter was reprobbed with mouse monoclonal antiactin antibody. The signal intensity of detected bands was quantified by NIH ImageJ 1.40 after normalization with actin.

Metabolic Stability. Test compounds in duplicate at the final concentration of 1 μM were dissolved in DMSO and preincubated for 10 min at 37 °C in potassium phosphate buffer (pH 7.4) containing 3 mM MgCl₂. The rat liver microsomes (Xenotech) were at a final concentration of 0.5 mg/mL. After the preincubation period, reactions were started by adding the cofactors mixture (NADP, glucose-6-phosphate, glucose-6-phosphate dehydrogenase). Samples were taken at times 0, 5, 10, 15, 20, and 30 min and added to acetonitrile to stop the reaction, and the timed samples were centrifuged. Supernatants were analyzed and quantified by LC-MS/MS. A control sample without cofactors was always added in order to check the stability of test compounds in the reaction mixtures. 7-Ethoxycoumarin and propranolol were used as a reference standards. A fixed concentration of verapamil was added in every sample as an internal standard for LC-MS/MS.

Samples were analyzed on a UPLC (Waters) interfaced with a Premiere XE Triple Quadrupole (Waters). Eluents were as follows: phase A: 95% H₂O, 5% acetonitrile + 0.1% HCOOH; phase B: 5% H₂O, 95% acetonitrile + 0.1% HCOOH. Flow rate, 0.6 mL/min; column, Acquity BEH C18, 50 \times 2.1 mm, 1.7 μm at 50 °C; injection volume, 5 μL . Samples were analyzed under the following conditions: electron spray ionization positive, desolvation temperature 450 °C, capillary 3.5 kV, extractor 5 V. The percent of test compound remaining after a 30 min incubation period was calculated from the peak area relative to the area of the compound at time zero.

Aqueous Solubility. The solubility of compound 5 was measured by means of the HTS. Samples were placed in a 96-well filter plate and incubated at room temperature for 90 min. The plate was then filtered, and solutions were analyzed by LC/MS-UV.

In Vivo Drug Pharmacokinetic Studies. Pharmacokinetic experiments were performed using 4 week old male nude CD-1 mice (Charles River Laboratories). Animals were quarantined for approximately 1 week prior to the study. They were housed under standard conditions and had free access to water and a standard laboratory rodent diet. Compound 5 was dissolved in a mixture of 3% DMSO + 30% PEG400 + NaCl 0.9% at the concentration for iv (rapid bolus) administration or a mixture of 5% DMSO + 20% PEG400 + water for the oral (gavage) dose (dose volume 5 mL/kg). Compound 5 was administered to mice either by the iv or the oral route, and blood samples were collected after different time points after dosing. Plasma was separated immediately after blood sampling by centrifugation, plasma proteins were precipitated using Sirocco filtration plates or Oasis HLB elution plates according to the distributor's instructions, and the plasma samples were kept frozen at -80 °C until LC/MS/MS analysis. Sample analysis was performed on an Acquity UPLC using either a Acquity BEH C18 column (50 mm \times 2.1 mm \times 1.7 μm) or a Acquity HSS T3 column (50 mm \times 2.1 mm \times 1.8 μm), coupled with a sample organizer and interfaced to a triple quadrupole Premiere XE (Waters). The mass spectrometer was

operated using an electrospray interface (ESI) with a capillary voltage of 3–4 kV, a cone voltage of 25–52 V, a source temperature of 115–120 °C, a desolvation gas flow of 800 L/h, and a desolvation temperature of 450–480 °C. The collision energy was optimized for each compound. LC–MS/MS analyses were carried out using a positive electrospray ionization interface in multiple reaction monitoring mode. Pharmacokinetic parameters were calculated by a noncompartmental method using WinNolin 5.1 software (Pharsight).

Statistical Analysis. Data were analyzed using Prism 4.0 (GraphPad Software, Inc.). Results are expressed as mean \pm SEM.

■ ASSOCIATED CONTENT

■ Supporting Information

Additional chemical and biological material. This material is available free of charge via the Internet at <http://pubs.acs.org>.

■ AUTHOR INFORMATION

Corresponding Author

*Phone +39 06 4991 3800. Fax +39 06 4991 3133. E-mail: romano.silvestri@uniroma1.it.

■ ACKNOWLEDGMENTS

This research was supported by PRIN 2008 Grant No. 200879X9N9, and Progetti di Ricerca di Università, Sapienza Università di Roma. A.C. thanks Istituto Pasteur—Fondazione Cenci Bolognetti for his Borsa di Studio per Ricerche in Italia.

■ ABBREVIATIONS USED

MT, microtubule; ATI, arylthioindole; CSA4, combretastatin A-4; VBL, vinblastine; PTX, paclitaxel; VBR, vinorelbine; SAR, structure–activity relationship; MW, microwave; Pmax, maximum pressure; PPA, polyphosphoric acid; TBAF, tetrabutylammonium fluoride; MI, mitotic index; DAMA-colchicine, *N*-deacetyl-*N*-(2-mercaptoacetyl)colchicine; DAPI, 4',6-diamidino-2-phenylindole; Pgp, P-glycoprotein; FBS, fetal bovine serum; PFA, paraformaldehyde

■ REFERENCES

- (1) Bhalla, K. N. Microtubule-targeted anticancer agents and apoptosis. *Oncogene* **2003**, *22*, 9075–9086.
- (2) Jordan, M. A.; Wilson, L. Microtubules as a target for anticancer drugs. *Nat. Rev. Cancer* **2004**, *4*, 253–265.
- (3) Teicher, B. A. Newer cytotoxic agents: attacking cancer broadly. *Clin. Cancer Res.* **2008**, *14*, 1610–1617.
- (4) Honore, S.; Pasquier, E.; Braguer, D. Understanding microtubule dynamics for improved cancer therapy. *Cell. Mol. Life Sci.* **2005**, *62*, 3039–3056.
- (5) Bhattacharyya, B.; Panda, D.; Gupta, S.; Banerjee, M. Anti-mitotic activity of colchicine and the structural basis for its interaction with tubulin. *Med. Res. Rev.* **2008**, *28*, 155–183.
- (6) Ravelli, R. B.; Gigant, B.; Curmi, P. A.; Jourdain, I.; Lachkar, S.; Sobel, A.; Knossow, M. Insight into tubulin regulation from a complex with colchicine and a stathmin-like domain. *Nature* **2004**, *428*, 198–202.
- (7) Lin, M. C.; Ho, H. H.; Pettit, G. R.; Hamel, E. Antimitotic natural products combretastatin A-4 and combretastatin A-2: studies on the mechanism of their inhibition of the binding of colchicine to tubulin. *Biochemistry* **1989**, *28*, 6984–6991.
- (8) Nogales, E.; Whittaker, M.; Milligan, R. A.; Downing, K. H. High-resolution model of the microtubule. *Cell* **1999**, *96*, 79–88.
- (9) Nettles, J. H.; Li, H.; Cornett, B.; Krahn, J. M.; Snyder, J. P.; Downing, K. H. The binding mode of epothilone A on alpha, beta-tubulin by electron crystallography. *Science* **2004**, *305*, 866–869.
- (10) Buey, R. M.; Calvo, E.; Barasoain, I.; Pineda, O.; Edler, M. C.; Matesanz, R.; Cerezo, G.; Vanderwal, C. D.; Day, B. W.; Sorensen, E. J.; Lopez, J. A.; Andreu, J. M.; Hamel, E.; Diaz, J. F. Cyclostreptin

binds covalently to microtubule pores and luminal taxoid binding sites. *Nat. Chem. Biol.* **2007**, *3*, 117–125.

(11) Sridhare, M.; Macapinlac, M. J.; Goel, S.; Verdier-Pinard, D.; Fojo, T.; Rothenberg, M.; Colevas, D. The clinical development of new mitotic inhibitors that stabilize the microtubule. *Anticancer Drugs* **2004**, *15*, 553–555.

(12) (a) Chen, S. M.; Meng, L. H.; Ding, J. New microtubule-inhibiting anticancer agents. *Exp. Opin. Invest. Drugs* **2010**, *19*, 329–343. (b) Harris, R.; Marx, G.; Gillett, M.; Kark, A.; Arunanth, S. Colchicine-induced bone marrow suppression: treatment with granulocyte colony-stimulating factor. *J. Emergency Med.* **2000**, *18*, 435–440. (c) Mundy, W. R.; Tilson, H. A. Neurotoxic effects of colchicine. *Neurotoxicology* **1990**, *11*, 539–547.

(13) Schmidt, M.; Bastians, H. Mitotic drug targets and the development of novel anti-mitotic anticancer drugs. *Drug Resist. Update* **2007**, *10*, 162–181.

(14) De Martino, G.; La Regina, G.; Coluccia, A.; Edler, M. C.; Barbera, M. C.; Brancale, A.; Wilcox, E.; Hamel, E.; Artico, M.; Silvestri, R. Arylthioindoles, potent inhibitors of tubulin polymerization. *J. Med. Chem.* **2004**, *47*, 6120–6123.

(15) De Martino, G.; Edler, M. C.; La Regina, G.; Coluccia, A.; Barbera, M. C.; Barrow, D.; Nicholson, R. I.; Chiosis, G.; Brancale, A.; Hamel, E.; Artico, M.; Silvestri, R. Arylthioindoles, potent inhibitors of tubulin polymerization. 2. Structure activity relationships and molecular modeling studies. *J. Med. Chem.* **2006**, *49*, 947–954.

(16) La Regina, G.; Edler, M. C.; Brancale, A.; Kandil, S.; Coluccia, A.; Piscitelli, F.; Hamel, E.; De Martino, G.; Matesanz, R.; Diaz, J. F.; Scovassi, A. I.; Prosperi, E.; Lavecchia, A.; Novellino, E.; Artico, M.; Silvestri, R. New arylthioindoles inhibitors of tubulin polymerization. 3. Biological evaluation, SAR and molecular modeling studies. *J. Med. Chem.* **2007**, *50*, 2865–2874.

(17) La Regina, G.; Sarkar, T.; Bai, R.; Edler, M. C.; Saletti, R.; Coluccia, A.; Piscitelli, F.; Minelli, L.; Gatti, V.; Mazzoccoli, C.; Palermo, V.; Mazzoni, C.; Falcone, C.; Scovassi, A. I.; Giansanti, V.; Campiglia, P.; Porta, A.; Maresca, B.; Hamel, E.; Brancale, A.; Novellino, E.; Silvestri, R. New arylthioindoles and related bioisosteres at the sulfur bridging group. 4. Synthesis, tubulin polymerization, cell growth inhibition, and molecular modeling studies. *J. Med. Chem.* **2009**, *52*, 7512–7527.

(18) Ciapetti, P.; Giethlen, B. Molecular variations based on isosteric replacement. Carboxylic esters bioisosteres. In *The practice of medicinal chemistry*, 3rd ed.; Wermuth, C. G., Elsevier Ltd: Oxford, U.K., 2008; pp 310–313.

(19) Hugon, B.; Pfeiffer, B.; Renard, P.; Prudhomme, M. Synthesis of isogranulatimide analogues possessing a pyrrole moiety instead of an imidazole heterocycle. *Tetrahedron Lett.* **2003**, *44*, 3927–3930.

(20) Bergman, J.; Venemalm, L. Efficient synthesis of 2-chloro-, 2-bromo-, and 2-iodoindole. *J. Org. Chem.* **1992**, *57*, 2495–2497.

(21) Bartoli, G.; Bosco, M.; Dalpozzo, R.; Todesco, P. E. Functionalization of aromatic systems: a highly chemoselective synthesis of trimethylsilyl-methylnitroarenes. *J. Org. Chem.* **1986**, *51*, 3694–3696.

(22) Shi, J.; Orth, J. D.; Mitchison, T. Cell type variation in responses to antimitotic drugs that target microtubules and kinesin-5. *Cancer Res.* **2008**, *68*, 3269–3276.

(23) Gascoigne, K. E.; Taylor, S. S. Cancer cells display profound intra- and interline variation following prolonged exposure to antimitotic drugs. *Cancer Cell* **2008**, *14*, 111–122.

(24) Sudakin, V.; Yen, T. G. Targeting mitosis for anti-cancer therapy. *BioDrugs* **2007**, *21*, 225–233.

(25) Gascoigne, K. E.; Taylor, S. S. How do anti-mitotic drugs kill cancer cells? *J. Cell Sci.* **2009**, *122*, 2579–2585.

(26) Vitale, I.; Galluzzi, L.; Castedo, M.; Kroemer, G. Mitotic catastrophe: a mechanism for avoiding genomic instability. *Nat. Rev. Mol. Cell. Biol.* **2011**, *12*, 385–392.

(27) (a) Impens, F.; Van Damme, P.; Demol, H.; Van Damme, J.; Vandekerckhove, J.; Gevaert, K. Mechanistic insight into taxol-induced cell death. *Oncogene* **2008**, *27*, 4580–4591. (b) McGrogan, B. T.; Gilmartin, B.; Carney, D. N.; McCann, A. Taxanes, microtubules and

chemoresistant breast cancer. *Biochim. Biophys. Acta* **2008**, *2*, 96–132.

(c) Mollinedo, F.; Gajate, C. Microtubules, microtubule-interfering agents and apoptosis. *Apoptosis* **2003**, *8*, 413–450.

(28) Kerns, E. H.; Di, L. Plasma stability methods. In *Drug-like properties: concepts, structure design and methods*; Academic Press: Burlington, MA, 2008; pp 329–347.

(29) Kraus, G. A.; Guo, H. One-pot synthesis of 2-substituted indoles from 2-aminobenzyl phosphonium salts. A formal total synthesis of arcyriacyanin A. *Org. Lett.* **2008**, *10*, 3061–3063.

(30) An alternative preparation of **26** was recently described: Ostrowski, T.; Golankiewicz, B.; De Clercq, E.; Andrei, G.; Snoeck, R. Synthesis and anti-VZV activity of 6-heteroaryl derivatives of tricyclic acyclovir and 9- $\{$ cis-1',2'-bis(hydroxymethyl)cycloprop-1'-yl $\}$ methyl $\}$ guanidine analogues. *Eur. J. Med. Chem.* **2009**, *44*, 3313–3317.

(31) Hudkins, R. L.; Diebold, J. L.; Marsh, F. D. Synthesis of 2-aryl- and 2-vinyl-1*H*-indoles via palladium-catalyzed cross-coupling of aryl and vinyl halides with 1-carboxy-2-(tributylstannyl)indole. *J. Org. Chem.* **1995**, *60*, 6218–6220.

(32) Fang, Y.-Q.; Lautens, M. A highly selective tandem cross-coupling of gem-dihaloolefins for a modular, efficient synthesis of highly functionalized indoles. *J. Org. Chem.* **2008**, *73*, 538–549.

(33) Caubere, C.; Caubere, P.; Ianelli, S.; Nardelli, M.; Jamart-Gregoire, B. Aggregative activation and heterocyclic chemistry. I. Complex base promoted arynic cyclization of imines or enamino ketones; regiochemical synthesis of indoles. *Tetrahedron* **1994**, *50*, 11903–11920.

(34) Hamel, E. Evaluation of antimetabolic agents by quantitative comparisons of their effects on the polymerization of purified tubulin. *Cell Biochem. Biophys.* **2003**, *38*, 1–21.

(35) Verdier-Pinard, P.; Lai, J.-Y.; Yoo, H.-D.; Yu, J.; Marquez, B.; Nagle, D. G.; Nambu, M.; White, J. D.; Falck, J. R.; Gerwick, W. H.; Day, B. W.; Hamel, E. Structure-activity analysis of the interaction of curacin A, the potent colchicine site antimetabolic agent, with tubulin and effects of analogs on the growth of MCF-7 breast cancer cells. *Mol. Pharmacol.* **1998**, *35*, 62–76.

(36) Ferlini, C.; Raspaglio, G.; Mozzetti, S.; Cicchillitti, L.; Filippetti, F.; Gallo, D.; Fattorusso, C.; Campiani, G.; Scambia, G. The seco-taxane IDN5390 is able to target class III β -tubulin and to overcome paclitaxel resistance. *Cancer Res.* **2005**, *65*, 2397–2405.